PCCP

PAPER

View Article Online
View Journal

Cite this: DOI: 10.1039/d5cp03493k

Room temperature dynamics of atomic clusters adsorbed on graphene: a machine-learning force field molecular dynamics study

Ramasamy Murugesan, *[a] Ewald Janssens, [b] Joris Van de Vondel [b] and Michel Houssa*[ac]

Clusters adsorbed on graphene can alter the electronic and spin-based properties of this two-dimensional material by proximity interactions. However, at room temperature, the adsorbed clusters tend to move freely over the surface. First-principles molecular dynamics simulations are performed to study the motion of size-selected Au_n (n = 3 and 6) clusters adsorbed on the graphene surface. While the clusters are found to be diffusive along the surface of pristine graphene, the presence of C-vacancies in graphene drastically suppresses the diffusion of the clusters and ''anchors'' them to the vacancy site. Besides carbon vacancies, the presence of resist residues like methyl methacrylate, which is commonly used in the fabrication process of nanoscale devices, was also considered in this work. The presence of residues on the surface of graphene strongly reduces the diffusion of the Au_n clusters.

Received 10th September 2025,
Accepted 18th December 2025

DOI: 10.1039/d5cp03493k

rsc.li/pccp

Introduction

The study of two-dimensional materials has gained widespread interest in recent years for electronic and spintronic applications. Due to the extreme sensitivity of graphene to its environment, adsorbed adatoms, atomic clusters, or other 2D materials can serve as ideal tools to tailor its electronic properties through proximity interactions, without significantly altering its linear energy dispersion. The physical adsorption of adatoms can induce charge transfer and band gap opening in the electronic structure of graphene, by breaking its sublattice symmetry.[1–3] Besides charge redistribution, the adsorption of metal atoms and nanoparticles can (locally) enhance the spin–orbit coupling (SOC) of graphene, by means of proximity effects. To magnify the SOC, graphene can be functionalized by interfacing it with *e.g.* adatoms, various substrates, or transition metal dichalcogenides (TMD). The inherent lack of symmetry at the graphene and adatom/substrate/TMD interface enables the enhancement of interfacial SOC.[4–8]

In addition to adatoms, size-selected atomic clusters can modulate graphene's properties. One of the intriguing features of the clusters is that their properties strongly depend on their size and composition.[9–12] This leads to a unique atom-by-atom control over the induced physio-chemical and electronic properties in graphene. Srivastava *et al.* studied the doping characteristics of Au_n and Fe_n clusters adsorbed on perfect and defective graphene.[13] They observed a size-dependent charge transfer from the clusters to graphene, with the interaction being more pronounced in the presence of a graphene vacancy defect.

Supported metal clusters attract significant interest due to their size-dependent reactivity, fluxionality and potential use in atom-efficient catalysts. Recent efforts highlight how the interplay between cluster geometry, charge redistribution and the electronic structure of the support governs the catalytic performance.[14] A recent review emphasized that understanding adsorption energies, diffusion pathways and support-induced structural distortion is essential for establishing structure–reactivity relationships in metal cluster catalysis.[15] In this context, graphene provides a well-defined electronically tunable support on which the intrinsic behavior of small cluster can be probed.

Few recent experimental studies have been devoted to the study of the interaction of graphene with metallic clusters. In the work of Scheerder *et al.*, the first experimental demonstration of size-specific adsorption of gold clusters (comparing Au_3 and Au_6) on graphene has been reported.[16] From the electronic transport measurements, it was observed that the adsorbed gold clusters of different sizes dope graphene very differently.

[a] Semiconductor Physics Laboratory, Department of Physics and Astronomy, KU Leuven, Celestijnenlaan 200D, B-3001 Leuven, Belgium, ramasamy.murugesan@kuleuven.be, michel.houssa@kuleuven.be
[b] Quantum Solid-State Physics, Department of Physics and Astronomy, KU Leuven, Celestijnenlaan 200D, B-3001 Leuven, Belgium
[c] Imec, Kapeldreef 75, B-3001 Leuven, Belgium

Subsequently, Keijers *et al.*, fabricated a graphene nonlocal spin valve modified with Au_3 or Au_6 clusters, and performed Hanle spin precession measurements to study the enhanced spin–orbit interaction in graphene induced by the atomic clusters.[17] These studies highlight the size dependent effect of Au clusters absorbed on graphene, with a peculiar odd–even oscillation in their induced properties. Besides the induced electronic and magnetic properties in graphene, gold clusters were also studied for their chemical reactivity. Libeert *et al.*, explored the Au_3 adsorbed graphene system as a probe to study the adsorption and desorption kinetics of oxygen molecules on the gold clusters.[18] These works collectively underscore the emerging importance of atomically precise cluster–support interfaces.

Recent works on supported metal clusters emphasize that predictive modelling requires not only knowledge about the equilibrium adsorption configurations and also of the dynamical behavior of clusters on surfaces.[15] Libeert *et al.*[18] and Zarshenas *et al.*[19] showed that atomic clusters adsorbed on graphene can be quite mobile, *i.e.* at room temperature they can move along the surface of pristine graphene. In the recent work of Settem *et al.*[20] the potential energy surface of large Au nanocluster adsorbed on graphene/graphite were studied for predicting cluster diffusion pathways and pinning events. They observed a reduced barrier for pathways involving simultaneous rotation and translation. Similarly, a recent perspective on atomically precise cluster–support interfaces argues that accurate first-principles simulations are essential to capture the diffusion, and deformation effects of the cluster adsorbed on the support.[21]

Scheerder *et al.*[22] attempted to observe Au_3 clusters deposited on graphene using scanning electron microscopy (SEM), and they observed large, coalesced structures with a radius of about 3 nm. These large structures were estimated to account for approximately 30% of the total deposited gold.[23] Though 30% of the deposited clusters coalesce, the remaining 70% was assumed to remain dispersed; with the remark that those small clusters could not be imaged due to the resolution of the SEM setup. It is still unclear what might be causing this inhibition of the diffusion of a large fraction of the clusters. The graphene surface corrugation due to the Si/SiO_2 supporting substrate could be one of the reasons.[24] Another possible effect that could hinder the diffusion of the clusters is the presence of resist residues. Polymer chains like polymethyl methacrylate (PMMA) can be left on the graphene's surface during device processing, such as the transfer of graphene on Si/SiO_2 substrates, the etching of graphene, or during metal contact patterning. These PMMA residues could act as ''trapping sites'' and restrict the motion of the clusters.[25,26] Finally, the presence of vacancies in graphene has also been reported to suppress the motion of adsorbed atoms.[27]

In this work, first-principles molecular dynamics simulations are performed to study the diffusion dynamics of Au_n (n = 3 and 6) clusters on a freestanding graphene monolayer. The impact of C-vacancies and resist residues, specifically $C_5H_8O_2$ methyl methacrylate (MMA), a monomer of the PMMA polymer utilized in the nanofabrication process, are investigated for their influence on the motion of the clusters. The results from our simulations suggest that the Au_3 and Au_6 clusters are quite mobile on the surface of pristine graphene. The presence of resist residues is found to hinder the motion of the adsorbed clusters; the estimated diffusion coefficients of the clusters are indeed strongly reduced by the presence of MMA. The analysis of the cluster mean-square displacements indicates the sub-diffusion of the Au_n clusters on the graphene/MMA surface. But only in the presence of a carbon vacancy on the graphene's surface, the diffusion of the clusters is completely suppressed. The motion of the clusters is restricted near the vacancy site, which strongly ''anchors'' the cluster. The doping efficiency and the electronic structure of the cluster/graphene system are also altered by the presence of the C-vacancy.

Methods

The simulation results presented in this manuscript were performed using density functional theory (DFT), as implemented in the Vienna *ab initio* simulation package (VASP) with plane wave basis sets.[28–30] The ion core of the atoms was described using projector-augmented wave potential.[31] The structural relaxation calculations were performed using a 5 × 5 × 1 k-point mesh with an energy cut-off of 400 eV.[32] The structures were relaxed until the forces between the atoms were less than 25 meV $Å^{-1}$. The clusters were relaxed on a 5 × 5 graphene supercell to avoid interactions between the clusters. The z-axis of the supercell was set to 20 Å to prevent spurious interlayer interactions. The exchange and correlation part of the Hamiltonian was described using the generalized gradient approximation (GGA) as developed by Perdew, Burke, and Ernzerhof (PBE).[33] To account for the van der Waals interactions (vdW), a dispersion correction term (DFT-D3) of Grimme *et al.* with Becke–Johnson damping function was used.[34–36] To validate the PBE-D3(DJ) description of the Au clusters-graphene interaction, the Au_2-coronene interaction energy curve was benchmarked against DLPNO-CCSD(T), using a procedure adopted in ref. 37 and 38. PBE-D3(BJ) underestimates the binding energy by ∼0.33 eV but it accurately reproduces the shape of the curve, equilibrium distance (≈2.31 Å), and the site-dependent corrugation of the potential energy surface (see SI for more details).

Molecular dynamics (MD) simulations were performed using ''on-the-fly training'' of machine learning (ML) force fields, as implemented in VASP.[39–41] MD simulations were done on (5 × 5) graphene supercells within the canonical ensemble (NVT) using the Nosé–Hoover thermostat, with the temperature set to 300 K.[42–44] The trajectories of the systems were computed for 1 ns with a time step of 1 fs for the pristine cluster/graphene systems and the graphene with a single C-vacancy in a 5 × 5 supercell. For the cluster/graphene systems with an MMA monomer, the time step was fixed to 0.5 fs, because the presence of H atoms with lighter nuclei requires the use of a reduced time step. The results obtained from the MD

simulations were further processed using VASPKIT and MDAnalysis, to extract the quantities of interest.[45–47]

The binding energy (BE) of the clusters on graphene was calculated using the following equation

$$\mathrm{BE} = E_{\mathrm{g+M_n}} - E_{\mathrm{g}} - E_{\mathrm{M_n}}, \quad (1)$$

where $E_{\mathrm{g+M_n}}$ is the total energy of the cluster adsorbed graphene, E_{g} is the energy of pristine graphene, and $E_{\mathrm{M_n}}$ is the energy of an isolated cluster with n atoms. All energies were obtained after full geometrical optimization without imposing any structural constraints. To obtain the electronic structure for the ground state configuration of the graphene/Au_n system, the Brillouin zone was sampled with a denser mesh of $13 \times 13 \times 1$ k-points. The width of the Gaussian smearing for the occupation of electronic levels was set to 0.05 eV to obtain the band structures.

Results and discussion

Clusters adsorbed on pristine graphene

To access the room temperature dynamics of the Au_n clusters absorbed on graphene, the starting structural configuration is obtained by performing DFT-based geometrical relaxation. The lowest energy configuration for the absorbed clusters is obtained by relaxing the entire structure: Au_n clusters are relaxed in all possible configurations to obtain the equilibrium configuration. The Au_3 cluster prefers to adsorb on a C–C bridge position with a binding energy of −1.06 eV. The Au–C bond lengths are about 2.25 Å and 2.52 Å. The adsorption of the Au_3 cluster on graphene slightly distorts the C–C bond length: the C–C bond length between the anchor carbon atoms is increased by 0.025 Å, and its nearest neighbour bond length is distorted by 0.01–0.02 Å. The Au_6 cluster prefers to align parallel to the graphene plane at a distance of about 3.4 Å, with an estimated binding energy of −1.19 eV.[17,48] In addition, the Au_6 cluster adsorption does not result in significant distortion of the graphene plane. In their lowest energy configuration, the Au atoms of the Au_6 cluster are located above hollow sites of the graphene honeycomb lattice. Electronic structure calculations were also performed to determine the doping characteristic of the adsorbed cluster on graphene's electronic structure. The adsorbed Au_3 cluster leads to n-type doping of graphene, as observed from the shift of the Fermi level above the Dirac point, with an estimated doping efficiency of 0.033 e per cluster.[48] The predicted n-type doping for Au_3/graphene is in agreement with the experimental work of Scheerder *et al.*[16] and Keijers *et al.*[17]

However, experiments also indicate n-type doping for Au_6 clusters adsorbed on graphene, while the DFT simulations on Au_6 cluster adsorbed on pristine graphene do not yield any doping effect.[17,48] Possible reasons for the discrepancy could be due to substrate effects or the presence of defects; doping induced by a single carbon vacancy or (part of) the clusters coalescing into a larger structure, thereby resulting in a different doping behavior than predicted by DFT simulations. To address this issue, it is essential to first establish if the clusters are mobile on the surface of graphene. In later sections, we address how the presence of defects and "mobile" clusters could modify the density of states at the Fermi level.

The dynamics of the clusters on the freestanding pristine graphene layer is first investigated. DFT equilibrium atomic configurations for Au_3 and Au_6 clusters adsorbed on graphene[17,48] were chosen as the initial systems for the MD simulations. The migration profile of the clusters along the graphene surface is studied by following the trajectories of the cluster's center of mass (CM). Fig. 1 shows the trajectories of cluster's CM during the MD simulation, the red and grey circles

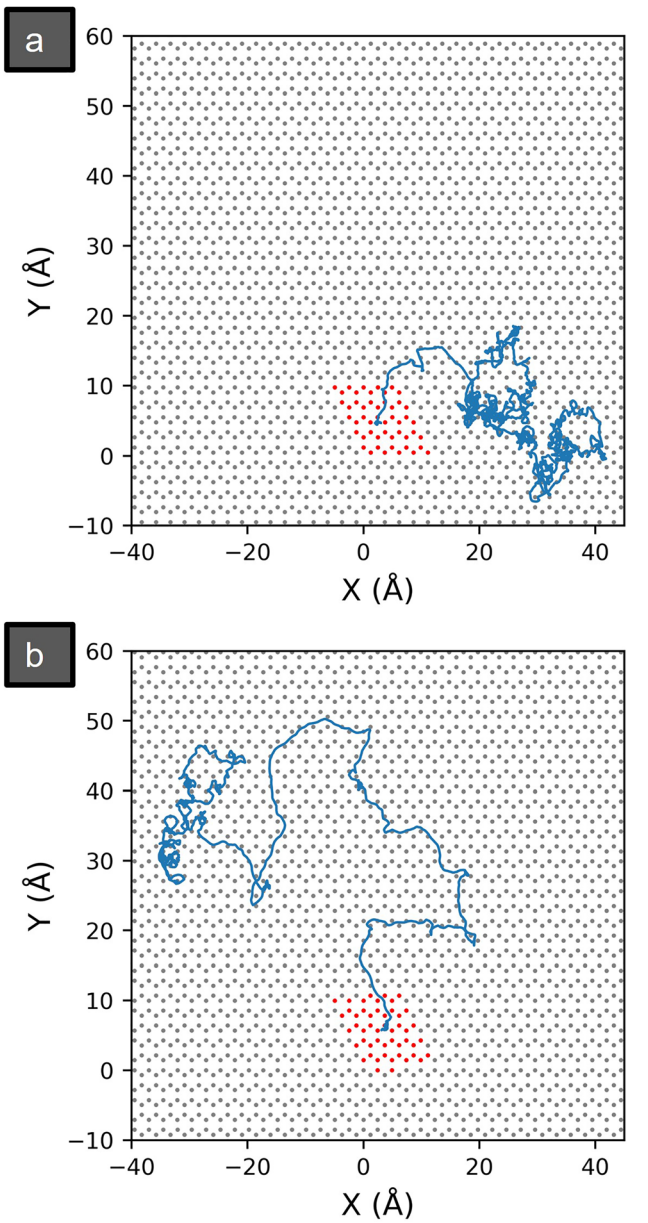

Fig. 1 Trajectories of Au_3 (a) and Au_6 (b) cluster's center of mass on pristine graphene during an MD simulation runs of 1 ns at 300 K. The red and grey circles denote the carbon atoms of the graphene sheet, with red ones indicating the initial 5×5 supercell utilized as the starting position for cluster adsorption.

indicates the position of carbon atoms of the graphene sheet. From this figure, it can be observed that the clusters are mobile at room temperature. After 1 ns, the Au_3 and Au_6 clusters move over 2D (XY) surfaces with areas of 9.9 nm^2 and 24.3 nm^2, respectively. The area was estimated from the maximum displacement of cluster trajectories in both the x and y directions, as presented in Fig. 1. The maximum displacements along the Z-axis, perpendicular to the graphene surface, are found to be in the range of $\sim$0.02 to 0.06 Å. Such short displacements indicate that the clusters remain adsorbed to the graphene surface during the simulation. The observed bigger spread of trajectories for the Au_6 cluster, in comparison with the Au_3 clusters, confirms that the interaction between the cluster and graphene depends on the size of the cluster.

To further understand the dynamics of the cluster, the mean square displacement (MSD) of the cluster was calculated, using the windowed MSD method,[25,45] where the MSD is averaged over all possible lag times (τ), as provided by the following relation,

$$\mathrm{MSD}(\tau) = \frac{1}{N}\sum_{n=0}^{N} |r(n\Delta t + \tau) - r(n\Delta t)|^2 \qquad (2)$$

where r are the coordinates of the center of mass of the cluster, Δt is the simulation time step and N is the number of sub-trajectories that fit within the total simulation time. The lag time corresponds to the duration of all the possible sub-trajectories that can be formed within the total trajectory. From this equation, the statistical significance of the computed MSD decreases for a longer lag time, as the number of sub-trajectories available for calculating MSD decreases. τ_{cut} = 50 ps was chosen to fit the MSD; based on the observed cluster trajectory in Fig. 1, this τ_{cut} corresponds to the time the cluster remains in the diffusion domain. To identify the diffusion process from the MSD plot, the following relation between MSD and diffusion constant was used,

$$\mathrm{MSD} = 4D\tau^{\beta} \qquad (3)$$

The power-law exponent β can be used to classify the diffusion process as subdiffusion ($\beta < 1$), normal diffusion ($\beta = 1$) or superdiffusion ($\beta > 1$).

The slope in the log–log plot of MSD *vs.* τ can be used to extract information regarding the diffusion process.[49,50] Fig. 2 presents a log–log plot of the MSD of the cluster's CM *vs.* τ, represented by a solid line. However, as shown in the work of Kepten *et al.*,[51] the slope of the curve is not constant, and it depends on the selected time interval for the fit. This variability can affect the interpretation of the diffusion dynamics in the system. Therefore, the linear fit of the curve was performed over multiple time intervals [0: τ], with $0 < \tau \leq 50$ ps. The probability distribution histogram of the extracted slope β of the MSD *vs.* τ curve is plotted in the insets of Fig. 2. Generally, as $\tau \to \infty$, the slope values dictate the diffusion process, therefore within the context of this work, the slope at 50 ps is used to identify the diffusion process. The corresponding fit to the MSD plot at τ = 50 ps timescale is provided in Fig. 2, where

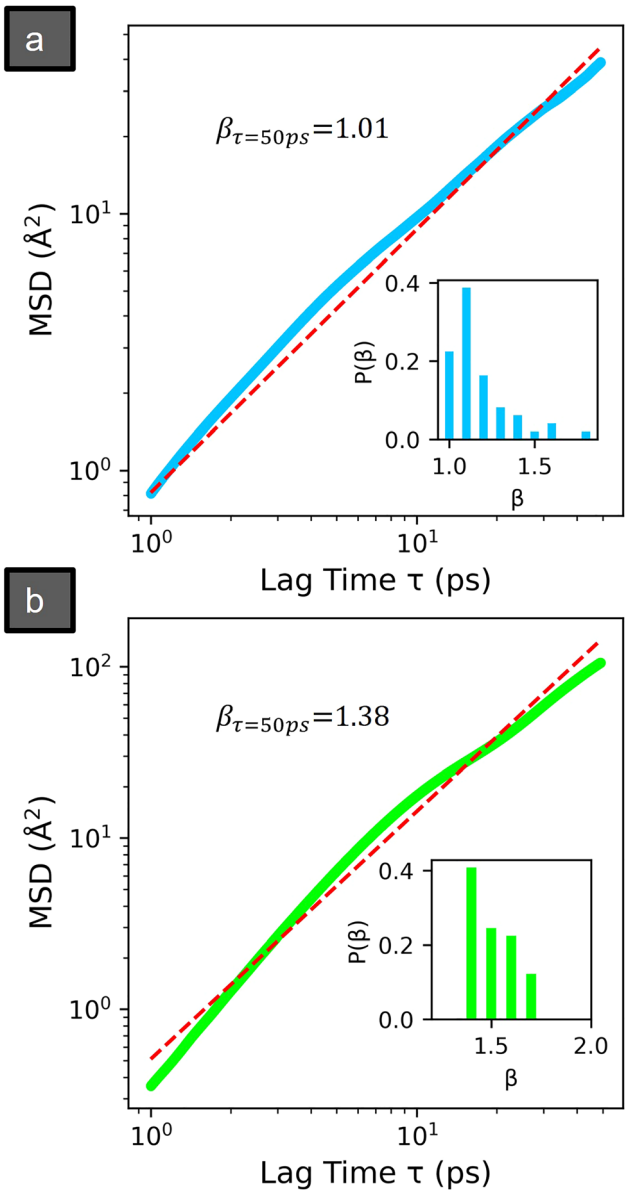

Fig. 2 Log–log plot of MSD *vs.* lag time, with the red dashed lines representing a power law fit with eqn (3) obtained at τ_{max} = 50 ps for Au_3 (a) and Au_6 (b). The probability distribution histogram of the extracted slope β for multiple time interval [0: τ] as computed from the trajectories in Fig. 1.

the red-dashed line corresponds to the fit. In the case of the Au_3 cluster (Fig. 2(a)), $\beta \approx 1.01$ is obtained. This suggests that the diffusion of the Au_3 cluster on the graphene surface is in normal-diffusive behavior. The probability distribution histogram shown in the inset also resulted in a value of $\beta \approx 1.1$ suggesting a normal-diffusive behavior. Whereas, in the case of the Au_6 cluster (Fig. 2(b)), $\beta \approx 1.38$, thereby suggesting a super-diffusive behavior. This can be correlated to the trajectories plot in Fig. 1(b), where the trajectories are composed of pieces of directed motion that connect domains of random walks. The probability distribution histogram of the slope β for Au_6 cluster consistently exhibits values exceeding 1, with the most

probable value being 1.4. This observation further supports the classification of super diffusive behaviour for the Au_6 cluster adsorbed on graphene. We speculate that the superdiffusive behaviour of the Au_6 cluster could be related to its adsorption geometry and interaction strength. The Au_6 cluster is located at 3.4 Å above graphene, and no significant distortion of the graphene layer is observed. Its planar structure effectively "floats" above graphene, enabling to reduce the energy barrier for diffusion and resulting in a super-diffusive behaviour.

Clusters adsorbed on graphene with a carbon vacancy

Based on the results obtained from the MD simulations, it is very likely that the clusters are mobile on the surface of single layer graphene. The presence of a single carbon vacancy (SV) in graphene is expected to result in a much stronger binding energy with the atomic clusters.[52] The SV could then act as an anchor site for the cluster adsorption, which restricts its diffusion. Initially, geometrical relaxations were performed on Au_3 and Au_6 clusters adsorbed on SV graphene. As shown in (SI S1), the clusters prefer to adsorb at the vacancy site. Note that upon relaxation, the geometry of the Au_6 cluster is deformed. The "anchoring" Au atom of the cluster is pulled closer to the defect site (Au–C ~2 Å), thereby significantly deforming the planar geometry of the Au_6 cluster. Similar to the results on Cu clusters reported in ref. 52, the Au clusters also exhibit a much stronger interaction with defective graphene. The binding energies of the clusters on SV graphene are compared in Table 1. Based on these computed values, the presence of the C vacancy likely results in the chemisorption of the clusters on graphene.

The presence of a single carbon vacancy in graphene alters its electronic structure and produces localized states within the band gap.[53] Fig. 3 shows the projected density of states (PDOS) of SV graphene's p_z states upon Au_3 and Au_6 cluster adsorption. The adsorption of the cluster induces a charge transfer with SV graphene, resulting in the shift of the Dirac cone from the Fermi level. In the case of Au_3 cluster adsorption, the Fermi level lies within the valence band (similar to SV graphene[53]), but when compared to the PDOS of SV graphene, there is a downward shift of the Dirac cone (as shown by the arrows in Fig. 3), suggesting electron transfer from the cluster to the graphene, with a doping efficiency of 0.014 electrons per cluster, which is about two times larger than the experimentally extracted value (0.006 e per cluster) on single layer graphene without carbon vacancies.[17]

In the case of the Au_6 cluster adsorbed on defective graphene, there is no state at the Fermi level. However, the Dirac point of Au_6 adsorbed on defective graphene (as indicated by the arrow in Fig. 3 is shifted downwards in comparison to that

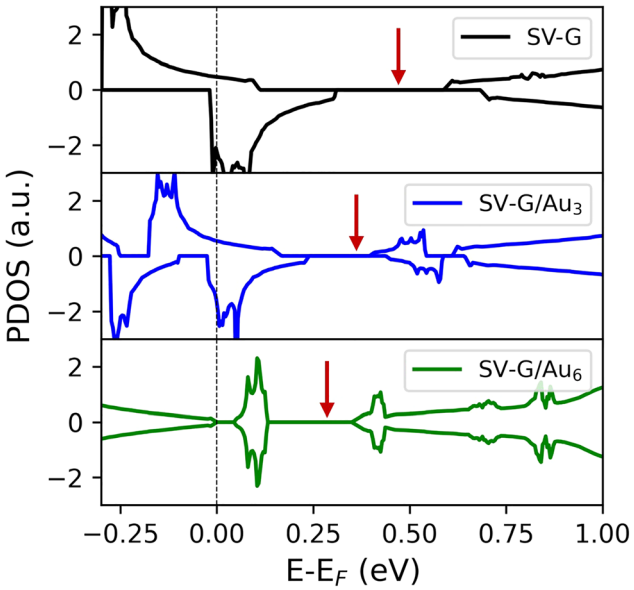

Fig. 3 The projected DOS (PDOS) of graphene p_z orbital states in SV graphene without clusters (black) and SV graphene with an absorbed Au_3 (blue) and Au_6 (green) cluster. The red arrows correspond to the positions of charge neutrality points in the different cases and the vertical dotted lines indicate the Fermi energies. The positive and and negative value correspond to the density of spin up and spin down states, respectively.

of SV graphene), indicating a negative shift in the charge neutrality point, when referenced with SV graphene. Based on the shift of the Dirac point, compared to SV graphene, we estimate a doping efficiency of 0.065 electron per cluster. The predicted value for doping efficiency is in good agreement with the (experimentally) estimated value of 0.08 electron per cluster by Keijers *et al.* for pristine graphene without carbon vacancies.[17]

The dynamics of the clusters adsorbed on SV graphene were next studied by performing MD simulations for 1 ns. The trajectories of the Au_n cluster's CM are plotted in Fig. 4. Both the Au_3 and Au_6 clusters are strongly confined to their adsorption site. The inset of Fig. 4 provides a view of the unit cell used in the computation; one can observe that the clusters remain close to the initial adsorption sites (*i.e.* the C-vacancy). The much stronger interaction between the Au clusters and SV graphene thus results in the restricted motion of the clusters near the vacancy site, which acts as a "trapping site" for the clusters. The clusters only exhibit pure rotational motion throughout the entire duration of the MD simulation, without any diffusional motion.

While carbon vacancies effectively restrict the motion of the clusters, it is unlikely that experiments[17,54] were performed solely on defective graphene. The presence of vacancies would modify the electronic structure of graphene, potentially negating some of the benefits derived from its linear dispersion. Therefore, we considered other possible defects which could restrict the diffusion of the clusters, without strongly modifying the Dirac cone. One possible candidate is a resist residue, resulting from the nanofabrication of functional graphene devices.

Table 1 Binding energies BE of Au_3 and Au_6 clusters adsorbed on pristine graphene, graphene with MMA residue, and graphene with a C-vacancy

Cluster	Pristine graphene (eV)	Graphene/$C_5H_8O_2$ (MMA) (eV)	Single C-vacancy (SV) graphene (eV)
Au_3	−1.06	−1.18	−4.20
Au_6	−1.19	−1.46	−3.34

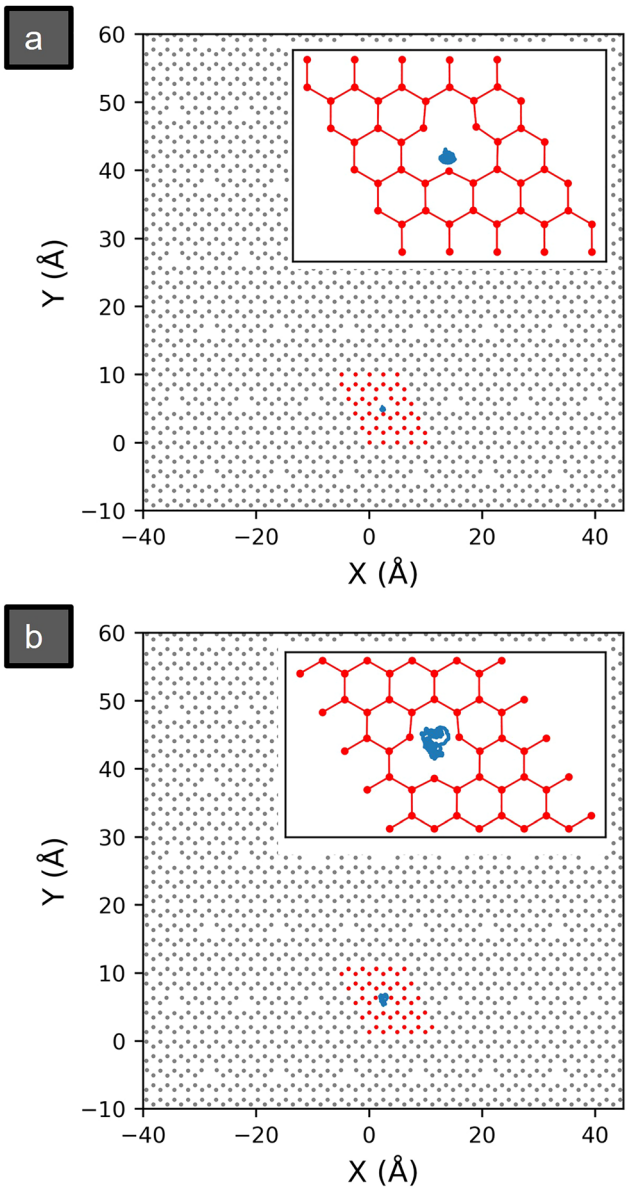

Fig. 4 The MD trajectories of Au_3 (a) and Au_6 (b) clusters adsorbed on graphene with a single carbon vacancy. The trajectories of the cluster remain confined at the adsorption site in the simulation unit cell as shown in the insets.

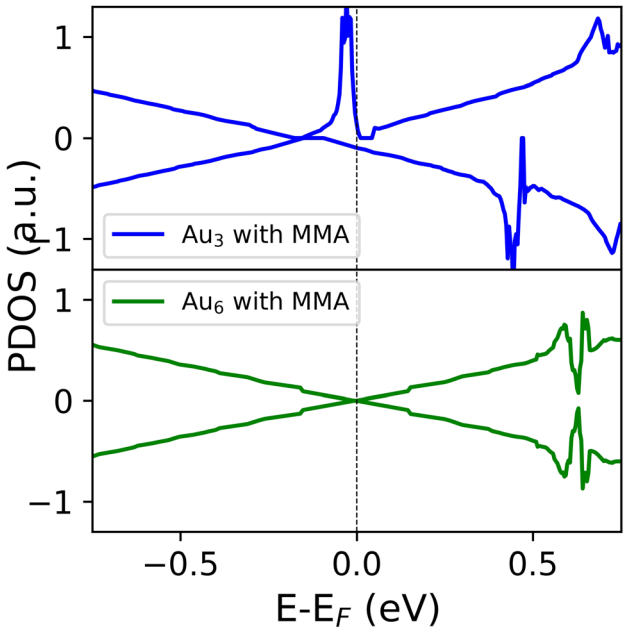

Fig. 5 The projected DOS (PDOS) of the graphene p_z orbital states for (blue) Au_3 and (green) Au_6 cluster/MMA/graphene.

Clusters adsorbed on MMA/graphene

The impact of MMA residues on the mobility of the clusters is next studied. To obtain the initial geometrical configurations for the MD simulations, structural relaxation calculations were performed on the cluster-adsorbed graphene surface with $C_5H_8O_2$ MMA residues at different locations. The obtained lowest energy configurations are shown in the inset of Fig. 6 for the Au_3 and Au_6 clusters.

The impact of the MMA residues on the electronic structure of the cluster/graphene systems was considered by computing the electronic density of states; the PDOS of graphene p_z orbital states are plotted in Fig. 5. The presence of the MMA residues does not lead to any significant doping of graphene, as no visible shift is observed in graphene's p_z orbital states. However, the presence of MMA residues slightly increases the binding energies of the clusters by 0.12 eV and 0.27 eV for the Au_3 and Au_6 clusters, respectively, as indicated in Table 1.

The DOS and binding energy calculations suggest that the presence of MMA residues could influence the diffusion of the clusters, without altering their electronic properties. The trajectories of the cluster's CM along the graphene surface with MMA residues are plotted in Fig. 6. Compared to pristine graphene/Au_n systems, in the presence of MMA residues Au clusters show reduced diffusion, with trajectories Au_3 and Au_6 clusters CM covering an area of 0.86 nm^2 and 1.36 nm^2, respectively. These smaller areas indicate that MMA residues significantly limit the movement of Au_3 and Au_6 clusters.

Since MMA residues suppress the motion of Au_n clusters on the graphene surface, they likely alter the diffusion mechanism of the clusters compared to that on pristine graphene. The log–log plot of MSD *vs.* τ is shown in Fig. 7 for Au_n clusters adsorbed on graphene with MMA residues. The slope values at τ_{cut} for Au_3 and Au_6 clusters were found to be 0.71 and 0.92, respectively, with their corresponding fit to MSD plot shown by red dotted lines. When compared to pristine graphene in Fig. 2, the slope in the presence of MMA residue is less than 1 at τ_{cut}, suggesting a sub-diffusive diffusion process for both clusters.

The probability distribution histogram of the extracted power law exponent β, shown in the inset of Fig. 7, further supports the observation of sub-diffusive behavior for both Au_3 and Au_6 clusters. In both cases, the most probable value of β is found to be less than 1. This indicates that, under the influence of MMA residues on the graphene surface, the diffusion of

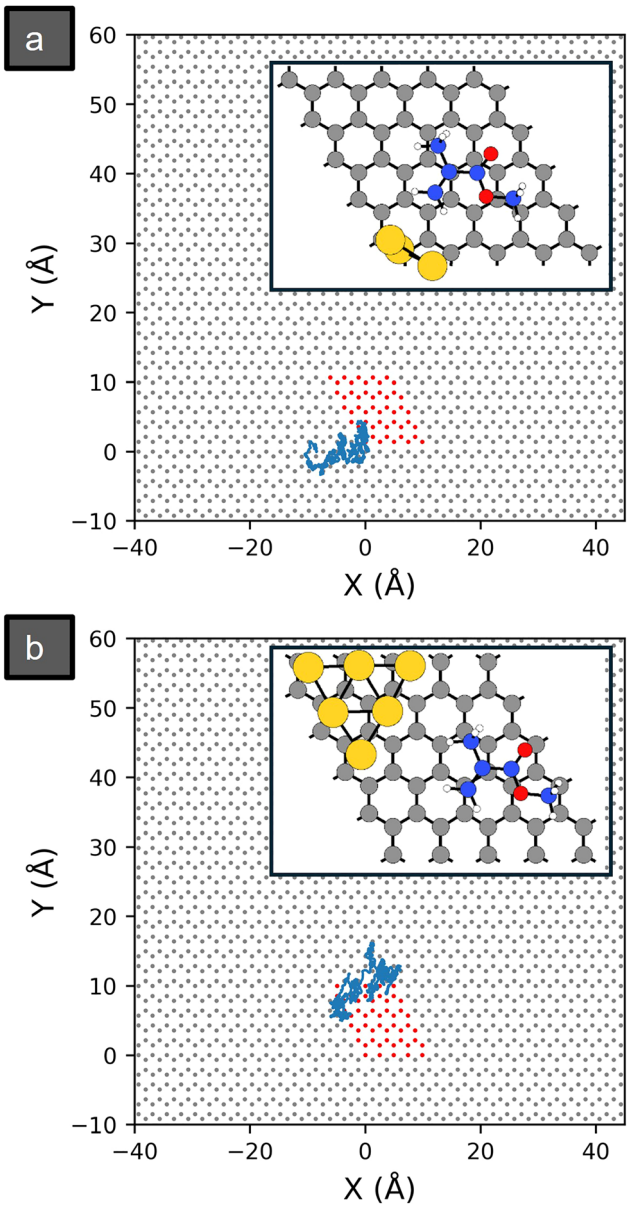

Fig. 6 The trajectories of Au_3 (a) and Au_6 (b) cluster's center of mass during the MD simulations on graphene surfaces with MMA residues. Inset: The relaxed geometrical configurations for Au_3 (a) and Au_6 clusters (b) adsorbed on graphene with $C_5H_8O_2$. The carbon atoms of MMA residues are shown in different colors.

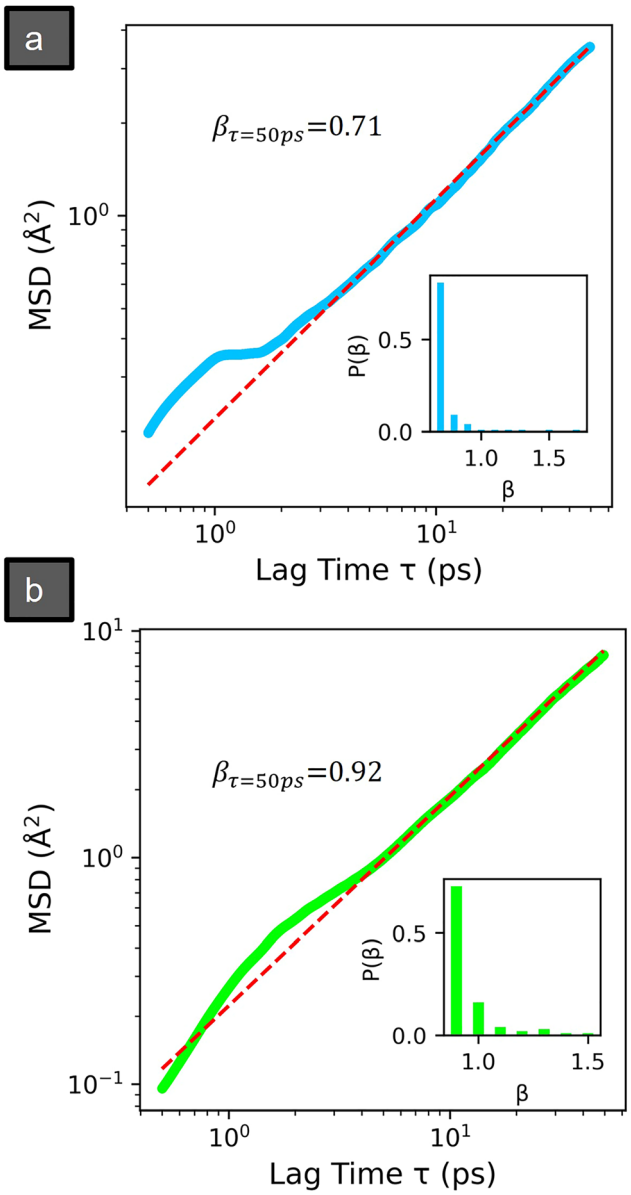

Fig. 7 Log–log plot of MSD *vs.* lag time, with the red dashed line representing the power law fit obtained at τ_{max} = 50 ps for Au_3 (a) and Au_6 (b) clusters absorbed on graphene layers with MMA residues. The probability distribution histogram of the extracted slope β for multiple time interval [0: τ] as computed from trajectories in Fig. 6.

these Au_n clusters is suppressed, and follows a sub-diffusive process. To address the reliability of our conclusion that the presence of MMA residues reduces the diffusion of the Au_n clusters, we repeated the simulations on a 10 × 5 graphene supercell. The slope value at τ_{cut} was found to be 0.705, with the most probable value of 0.8, in good agreement with the results obtained for the smaller supercell (SI S5). The consistent observation of a β values less than 1 for both cluster sizes reinforce the conclusion that MMA residues significantly restrict the movement of the Au_n clusters, when compared to the pristine graphene without any defects/impurities.

Note that the MMA residues are also mobile on the graphene surface (SI S2). Further analysis of the MD trajectories indicates a correlation between the motion of the MMA residues and the Au_n clusters, both remaining in the vicinity of each other. The distance between the CM of cluster and MMA residue remains almost constant throughout the entire MD simulation (SI S3). The MMA residues act as an "obstacle" to the cluster motion, thereby making the cluster motion sub diffusive. Note that the clusters could interact with the MMA residues to form metal–organic complexes, and the induced properties of graphene would be further modified by such complexes. Although the production of these metal–organic complexes was not observed

within the computed time scale, these reactions could certainly occur at larger timescales.

Conclusions

Molecular dynamics simulations have been performed to study the room temperature dynamics of Au_n (n = 3, 6) clusters on different single layer graphene surfaces: pristine graphene, graphene with a carbon vacancy, and graphene with MMA residue. Our results indicate that the clusters move nearly freely over the surface of pristine graphene. The clusters could thus diffuse and coalesce to form larger aggregates on graphene.

Defects, such as carbon vacancies, are found to ''anchor'' the Au_n clusters, strongly suppressing their motion on the graphene's surface. This finding could benefit the studies aiming to investigate the chemical reactivity of the clusters, which remain trapped to the vacancy sites. Since carbon vacancies can be formed on graphene by the bombardment with *e.g.* Ar ions, prior to the cluster adsorption,[23] they could be used to anchor the clusters.

In addition to vacancies, the presence of contaminants such as methyl methacrylate (MMA) resist residues is found to significantly reduce the motion of the clusters, suppressing their diffusion coefficients by an order of magnitude compared to pristine graphene. The reduction of the cluster mobility is likely related to the observed correlated motion between the clusters and residues from the MD simulations, which requires further studies. Interestingly, while these residues restrict cluster diffusion, they do not appear to significantly affect the clusters' electronic interactions with the graphene substrate. Such unintentional residues may thus inadvertently aid in immobilizing the clusters. This insight suggests that the motion of the cluster could be ''controlled'' through the introduction of impurities that do not chemically react with graphene, offering a potential strategy for experimental design.

Conflicts of interest

There are no conflicts to declare.

Data availability

The results presented in this work were performed using Vienna *ab initio* simulation package (VASP). The DFT optimized structure, which was the starting structure for MD simulation is provided with the supplementary information (SI). Supplementary information is available. See DOI: https://doi.org/10.1039/d5cp03493k.

Acknowledgements

This work has been financially supported by the KU Leuven Research Fund, project C14/21/083. Part of the computational resources and services used in this work have been provided by the VSC (Flemish Supercomputer Center), funded by the Research Foundation-Flanders (FWO) and the Flemish Government-department EWI.

Notes and references

1 R. Chen, F. Luo, Y. Liu, Y. Song, Y. Dong, S. Wu, J. Cao, F. Yang, A. N'Diaye, P. Shafer, Y. Liu, S. Lou, J. Huang, X. Chen, Z. Fang, Q. Wang, D. Jin, R. Cheng, H. Yuan, R. J. Birgeneau and J. Yao, Tunable room-temperature ferromagnetism in Co-doped two-dimensional van der Waals ZnO, *Nat. Commun.*, 2021, **12**, 3952.

2 K. Pi, K. M. McCreary, W. Bao, W. Han, Y. F. Chiang, Y. Li, S.-W. Tsai, C. N. Lau and R. K. Kawakami, Electronic doping and scattering by transition metals on graphene, *Phys. Rev. B: Condens. Matter Mater. Phys.*, 2009, **80**, 075406.

3 M. Papagno, S. Rusponi, P. M. Sheverdyaeva, S. Vlaic, M. Etzkorn, D. Pacilé, P. Moras, C. Carbone and H. Brune, Large Band Gap Opening between Graphene Dirac Cones Induced by Na Adsorption onto an Ir Superlattice, *ACS Nano*, 2012, **6**, 199–204.

4 I. Žutić, A. Matos-Abiague, B. Scharf, H. Dery and K. Belashchenko, Proximitized materials, *Mater. Today*, 2019, **22**, 85–107.

5 J. F. Sierra, J. Světlík, W. Savero Torres, L. Camosi, F. Herling, T. Guillet, K. Xu, J. S. Reparaz, V. Marinova, D. Dimitrov and S. O. Valenzuela, Room-temperature anisotropic in-plane spin dynamics in graphene induced by $PdSe_2$ proximity, *Nat. Mater.*, 2025, **24**, 876–882.

6 J. F. Sierra, J. Fabian, R. K. Kawakami, S. Roche and S. O. Valenzuela, van der Waals heterostructures for spintronics and opto-spintronics, *Nat. Nanotechnol.*, 2021, **16**, 856–868.

7 K. Zollner, S. M. João, B. K. Nikolić and J. Fabian, Twist- and gate-tunable proximity spin-orbit coupling, spin relaxation anisotropy, and charge-to-spin conversion in heterostructures of graphene and transition metal dichalcogenides, *Phys. Rev. B*, 2023, **108**, 235166.

8 M. Milivojević, M. Gmitra, M. Kurpas, I. Štich and J. Fabian, Giant asymmetric proximity-induced spin–orbit coupling in twisted graphene/SnTe heterostructure, *2D Mater.*, 2024, **11**, 035036.

9 R. Hussain, M. Saeed, M. Y. Mehboob, S. U. Khan, M. Usman Khan, M. Adnan, M. Ahmed, J. Iqbal and K. Ayub, Density functional theory study of palladium cluster adsorption on a graphene support, *RSC Adv.*, 2020, **10**, 20595–20607.

10 C. Jin, L. Cheng, G. Feng, R. Ye, Z.-H. Lu, R. Zhang and X. Yu, Adsorption of Transition-Metal Clusters on Graphene and N-Doped Graphene: A DFT Study, *Langmuir*, 2022, **38**, 3694–3710.

11 J. R. Rumptz, Z. Mao and C. T. Campbell, Size-Dependent Adsorption and Adhesion Energetics of Ag Nanoparticles on Graphene Films on Ni(111) by Calorimetry, *ACS Catal.*, 2022, **12**, 2888–2897.

12 T. Jadoon, K. Carter-Fenk, M. B. A. Siddique, J. M. Herbert, R. Hussain, S. Iqbal, J. Iqbal and K. Ayub, Silver clusters

tune up electronic properties of graphene nanoflakes: a comprehensive theoretical study, *J. Mol. Liq.*, 2020, **297**, 111902.

13 M. K. Srivastava, Y. Wang, A. F. Kemper and H.-P. Cheng, Density functional study of gold and iron clusters on perfect and defected graphene, *Phys. Rev. B: Condens. Matter Mater. Phys.*, 2012, **85**, 165444.

14 M. P. de Lara-Castells, C. Puzzarini, V. Bonačić-Koutecký, M. A. López-Quintela and S. Vajda, Stability and properties of new-generation metal and metal-oxide clusters down to subnanometer scale, *Phys. Chem. Chem. Phys.*, 2023, **25**, 15081–15084.

15 J. Jašík, A. Fortunelli and Š. Vajda, Exploring the materials space in the smallest particle size range: from heterogeneous catalysis to electrocatalysis and photocatalysis, *Phys. Chem. Chem. Phys.*, 2022, **24**, 12083–12115.

16 J. E. Scheerder, S. Liu, V. S. Zharinov, N. Reckinger, J.-F. Colomer, H.-P. Cheng, J. Van de Vondel and E. Janssens, Electronic Detection of Oxygen Adsorption and Size-Specific Doping of Few-Atom Gold Clusters on Graphene, *Adv. Mater. Interfaces*, 2018, **5**, 1801274.

17 W. Keijers, R. Murugesan, G. Libeert, J. E. Scheerder, B. Raes, S. Brems, S. De Gendt, M. Houssa, E. Janssens and J. Van, de Vondel, Tuning the spintronic properties of graphene with atomically precise Au clusters, *JPhys Mater.*, 2021, **4**, 045005.

18 G. Libeert, R. Murugesan, M. Guba, W. Keijers, S. Collienne, B. Raes, S. Brems, S. De Gendt, A. V. Silhanek, T. Höltzl, M. Houssa, J. Van de Vondel and E. Janssens, Au_3-Decorated graphene as a sensing platform for O_2 adsorption and desorption kinetics, *Nanoscale*, 2022, **14**, 12437–12446.

19 M. Zarshenas, V. Gervilla, D. G. Sangiovanni and K. Sarakinos, Room-temperature diffusion of metal clusters on graphene, *Phys. Chem. Chem. Phys.*, 2021, **23**, 13087–13094.

20 M. Settem, M. M. Gianetti, R. Guerra, N. Manini, R. Ferrando and A. Giacomello, Gold Clusters on Graphene/Graphite—Structure and Energy Landscape, *Small Sci.*, 2024, **4**, 2400078.

21 M. P. de Lara-Castells, An Ab Initio Journey toward the Molecular-Level Understanding and Predictability of Subnanometric Metal Clusters, *Small Struct.*, 2024, **5**(10), 2400147.

22 J. E. Scheerder, T. Picot, N. Reckinger, T. Sneyder, V. S. Zharinov, J.-F. Colomer, E. Janssens and J. Van, de Vondel, Decorating graphene with size-selected few-atom clusters: a novel approach to investigate graphene–adparticle interactions, *Nanoscale*, 2017, **9**, 10494–10501.

23 G. Libeert, E. Janssens and J. Van de Vondel, PhD thesis, Katholieke Universiteit Leuven, 2023.

24 L. Liu, Z. Chen, L. Wang, E. Polyakova (Stolyarova), T. Taniguchi, K. Watanabe, J. Hone, G. W. Flynn and L. E. Brus, Slow Gold Adatom Diffusion on Graphene: Effect of Silicon Dioxide and Hexagonal Boron Nitride Substrates, *J. Phys. Chem. B*, 2013, **117**, 4305–4312.

25 S. R. Plant, L. Cao, F. Yin, Z. W. Wang and R. E. Palmer, Size-dependent propagation of Au nanoclusters through few-layer graphene, *Nanoscale*, 2014, **6**, 1258–1263.

26 I. Lado-Touriño and A. Páez-Pavón, Interaction between Graphene-Based Materials and Small Ag, Cu, and CuO Clusters: A Molecular Dynamics Study, *Nanomaterials*, 2021, **11**, 1378.

27 D. Du, H. Zhu, Y. Guo, X. Hong, Q. Zhang, B. Suo, W. Zou and Y. Li, Anchoring Cu Clusters over Defective Graphene for Electrocatalytic Reduction of CO_2, *J. Phys. Chem. C*, 2022, **126**, 11611–11618.

28 G. Kresse and J. Hafner, Ab initio molecular dynamics for liquid metals, *Phys. Rev. B: Condens. Matter Mater. Phys.*, 1993, **47**, 558–561.

29 G. Kresse and J. Furthmüller, Efficiency of ab-initio total energy calculations for metals and semiconductors using a plane-wave basis set, *Comput. Mater. Sci.*, 1996, **6**, 15–50.

30 G. Kresse and D. Joubert, From ultrasoft pseudopotentials to the projector augmented-wave method, *Phys. Rev. B: Condens. Matter Mater. Phys.*, 1999, **59**, 1758–1775.

31 P. E. Blöchl, Projector augmented-wave method, *Phys. Rev. B: Condens. Matter Mater. Phys.*, 1994, **50**, 17953–17979.

32 H. J. Monkhorst and J. D. Pack, Special points for Brillouin-zone integrations, *Phys. Rev. B: Condens. Matter Mater. Phys.*, 1976, **13**, 5188–5192.

33 J. P. Perdew, K. Burke and M. Ernzerhof, Generalized Gradient Approximation Made Simple, *Phys. Rev. Lett.*, 1996, **77**, 3865–3868.

34 S. Grimme, S. Ehrlich and L. Goerigk, Effect of the damping function in dispersion corrected density functional theory, *J. Comput. Chem.*, 2011, **32**, 1456–1465.

35 S. Grimme, J. Antony, S. Ehrlich and H. Krieg, A consistent and accurate ab initio parametrization of density functional dispersion correction (DFT-D) for the 94 elements H-Pu, *J. Chem. Phys.*, 2010, **132**, 154104.

36 S. Grimme, Semiempirical GGA-type density functional constructed with a long-range dispersion correction, *J. Comput. Chem.*, 2006, **27**, 1787–1799.

37 M. P. de Lara-Castells, C. Cabrillo, D. A. Micha, A. O. Mitrushchenkov and T. Vazhappilly, *Ab initio* design of light absorption through silver atomic cluster decoration of TiO_2, *Phys. Chem. Chem. Phys.*, 2018, **20**, 19110–19119.

38 L. L. Carroll, L. V. Moskaleva and M. P. de Lara-Castells, Carbon vacancy-assisted stabilization of individual Cu_5 clusters on graphene. Insights from *ab initio* molecular dynamics, *Phys. Chem. Chem. Phys.*, 2023, **25**, 15729–15743.

39 R. Jinnouchi, F. Karsai, C. Verdi, R. Asahi and G. Kresse, Descriptors representing two- and three-body atomic distributions and their effects on the accuracy of machine-learned inter-atomic potentials, *J. Chem. Phys.*, 2020, **152**, 234102.

40 R. Jinnouchi, F. Karsai and G. Kresse, On-the-fly machine learning force field generation: application to melting points, *Phys. Rev. B*, 2019, **100**, 014105.

41 R. Jinnouchi, J. Lahnsteiner, F. Karsai, G. Kresse and M. Bokdam, Phase Transitions of Hybrid Perovskites Simulated by Machine-Learning Force Fields Trained on the Fly with Bayesian Inference, *Phys. Rev. Lett.*, 2019, **122**, 225701.

42 S. Nosé, Constant Temperature Molecular Dynamics Methods, *Prog. Theor. Phys. Suppl.*, 1991, **103**, 1–46.
43 S. Nosé, A unified formulation of the constant temperature molecular dynamics methods, *J. Chem. Phys.*, 1984, **81**, 511–519.
44 W. G. Hoover, Canonical dynamics: equilibrium phase-space distributions, *Phys. Rev. A: At., Mol., Opt. Phys.*, 1985, **31**, 1695–1697.
45 N. Michaud-Agrawal, E. J. Denning, T. B. Woolf and O. Beckstein, MDAnalysis: a toolkit for the analysis of molecular dynamics simulations, *J. Comput. Chem.*, 2011, **32**, 2319–2327.
46 R. Gowers, M. Linke, J. Barnoud, T. Reddy, M. Melo, S. Seyler, J. Domański, D. Dotson, S. Buchoux, I. Kenney and O. Beckstein, MDAnalysis: A Python package for the rapid analysis of molecular dynamics simulations, Proceedings of the 15th Python in Science Conference, 2016, pp. 98–105.
47 V. Wang, N. Xu, J.-C. Liu, G. Tang and W.-T. Geng, VASPKIT: a user-friendly interface facilitating high-throughput computing and analysis using VASP code, *Comput. Phys. Commun.*, 2021, **267**, 108033.
48 R. Murugesan, R. Meng, A. de Volder, W. Keijers, E. Janssens, J. van de Vondel, V. Afanasiev and M. Houssa, Interaction of graphene with Au_n clusters: a first-principles study, *J. Phys.: Condens. Matter*, 2022, **34**, 405701.
49 A. N. Kapanidis, S. Uphoff and M. Stracy, Understanding Protein Mobility in Bacteria by Tracking Single Molecules, *J. Mol. Biol.*, 2018, **430**, 4443–4455.
50 R. R. Ratnakar and B. Dindoruk, The Role of Diffusivity in Oil and Gas Industries: Fundamentals, Measurement, and Correlative Techniques, *Processes*, 2022, **10**, 1194.
51 E. Kepten, A. Weron, G. Sikora, K. Burnecki and Y. Garini, Guidelines for the Fitting of Anomalous Diffusion Mean Square Displacement Graphs from Single Particle Tracking Experiments, *PLoS One*, 2015, **10**, e0117722.
52 R. Murugesan, E. Janssens, J. Van de Vondel, V. Afanas'ev and M. Houssa, Tuning the spin texture of graphene with size-specific Cun clusters: a first-principles study, *JPhys Mater.*, 2023, **6**, 035005.
53 J.-J. Chen, H.-C. Wu, D.-P. Yu and Z.-M. Liao, Magnetic moments in graphene with vacancies, *Nanoscale*, 2014, **6**, 8814.
54 J. Scheerder, J. Van de Vondel and E. Janssens, PhD thesis, Katholieke Universiteit Leuven, 2018.

